


Yielding in an amorphous solid subject to constant stress at finite temperaturesHaiyan Xu ¹, Juan Carlos Andresen,² and Ido Regev ^{1,*}¹*Alexandre Yersin Department of Solar Energy and Environmental Physics, Jacob Blaustein Institutes for Desert Research, Ben-Gurion University of the Negev, Sede Boqer Campus 84990, Israel*²*Department of Physics, Ben Gurion University of the Negev, Beer Sheva 84105, Israel*

(Received 1 December 2020; accepted 22 April 2021; published 10 May 2021)

Understanding the nature of the yield transition is a long-standing problem in the physics of amorphous solids. Here we use molecular dynamics simulations to study the response of amorphous solids to constant stresses at finite temperatures. We compare amorphous solids that are prepared using fast and slow quenches and show that for thermal systems, the steady-state velocity exhibits a continuous transition from very slow creep to a finite strain rate as a function of the stress. This behavior is observed for both well-annealed and poorly annealed systems. However, the transient dynamics is different in the latter and involves overcoming an energy barrier. Due to the different simulation protocol, the strain rate as a function of stress and temperature follows a scaling relation that is different from the ones that are shown for systems where the strain is controlled. Collapsing the data using this scaling relation allows us to calculate critical exponents for the dynamics close to yield, including an exponent for thermal rounding. We also demonstrate that strain slips due to avalanche events above yield follow standard scaling relations and we extract critical exponents that are comparable to the ones obtained in previous studies that performed simulations of both molecular dynamics and elastoplastic models using strain-rate control.

DOI: [10.1103/PhysRevE.103.052604](https://doi.org/10.1103/PhysRevE.103.052604)**I. INTRODUCTION**

Understanding yield, the transition from elastic to plastic behavior, is of highest importance for modeling material strength. The importance of yield stems from the fact that in most technological devices it is important to avoid permanent deformation of machines and materials under mechanical loads and when such deformation occurs, it is of utmost importance to predict how the material will deform. Recently, there have been many indications that yield is a nonequilibrium phase transition [1–11]. However, the exact nature of this transition is still under debate. Specifically, it is still not clear if it is continuous or discontinuous and both scenarios have been suggested in the literature [1,4,9–14]. A discontinuous transition is traditionally associated with the formation of a shear band [12]. However, recently it was suggested in the context of crystal plasticity that a discontinuous transition may involve the nucleation of an unstrained particle configuration [15,16]. A continuous transition has been associated with a depinning or a depinninglike scenario [9,17,18]. Depinning has been suggested as a model for plastic deformation where one considers the displacement of the regions where plasticity occurs as displacements of an elastic manifold [18,19]. Contrary to the classical models of depinning of elastic manifolds, which usually involve short-range interactions, in depinning models of plasticity it is assumed that the interactions between the local displacements are long range with an Eshelby-like field (see detailed explanations in [9,17]).

A popular approach for studying the behavior of such systems is by molecular dynamics simulations. One of the main problems in studying the transition is that most of the numerical studies are performed under constant strain-rate conditions, either quasistatic, in which tiny strain steps are followed by energy minimization, or by applying a finite strain rate in which the material is being deformed continuously [20–22]. However, such a control scheme may cause the nature of the transition to become less obvious. A more natural control parameter, one that is commonly used in theories of plasticity and nonequilibrium phase transitions, such as depinning theory [18] and some elastoplastic models [17], is the force or stress. One important difference that was demonstrated for the dynamics under stress, compared to constant strain-rate dynamics, is that for small stresses the system eventually becomes arrested, while for large stresses the system flows at a constant strain rate, as has been recently demonstrated for granular materials [14,23]. For soft systems one can also expect creep, as has been observed recently [24]. While certain features of the transition under constant stress have been studied recently in simulations [14,23,24], the statistics of fluctuations and the nature of the transition (continuous vs discontinuous) have only partially been studied for athermal systems.

For systems subject to constant strain rates, the preparation protocol strongly affects the dynamics at yield. For solids prepared by a slow quench, a stress overshoot is typically observed, while the stress-strain curve of a material prepared by a fast quench is typically monotonic. We therefore expect that also under constant stress the preparation protocol will affect the nature of the yielding point. In solids prepared by

*Corresponding author: regevid@bgu.ac.il

a slow quench, once the system surpasses the stress at the stress peak, we expect it to immediately reach a finite strain rate. The behavior will thus be consistent with a discontinuous transition. For a solid prepared by a fast quench, we expect that as the applied stress approaches the steady-state stress there will be long transients which will become infinite at a critical stress, which is similar to the behavior observed in elastic manifolds undergoing depinning.

The shearing protocol may also have an effect on avalanche statistics, especially when compared to athermal, quasistatic, strain-controlled simulations. In the latter, the system is forced to reach mechanical equilibrium after each small strain step, which applies a very strict stopping condition for any avalanche that is developed due to an applied strain. In constant stress simulations, a subyield avalanche, triggered by an increase in the stress, will continue until it becomes arrested by the next energy barrier.

In this work we use molecular dynamics simulations to study the dynamics of amorphous solids subject to constant stresses at finite temperatures and show that the asymptotic value of the strain rate as a function of the stress exhibits behavior that is consistent with a continuous transition. However, we also show that the transient behavior leading to this steady state is affected by the quench protocol and that the transient dynamics in a solid that is prepared using a slow quench is consistent with overcoming a finite energy barrier, which may indicate a nucleation process typical of discontinuous transitions. We also obtain different critical exponents by studying the scaling of the strain rate and of avalanche statistics as a function of the applied stress and compare the values of these critical exponents to the values obtained from athermal quasistatic dynamics and elastoplastic models.

II. RESULTS

We perform molecular dynamics simulations in two dimensions of a 50:50 binary mixture of small and large particles with a size ratio of 1.4, interacting via a Lennard-Jones interaction potential. Initial configurations are prepared by quenching systems from the liquid state to near-zero temperatures. In order to probe the dependence on sample preparation we obtain 35 initial amorphous solids using different constant cooling rates from the liquid. These systems are then sheared using the thermostated algorithm of Parrinello and Rahman [25], which allows shearing at a constant stress, pressure, and temperature (see the Appendix for further details). We should note that we control the Cauchy stress rather than the Piola-Kirchhoff stress that is usually controlled in constant stress simulations [23,26]. We believe that the former is more relevant for simulations at finite strain rates and for that reason preferred to use it.

A. Stress and temperature dependence of the strain rate

To probe the nature of the transition we first study the strain rate as a function of the stress at the steady state at different temperatures and using several quenching protocols (see the Appendix). For initial configurations prepared using a fast quench, the strain rate at the steady state as a function of the applied stress is calculated for a system of $N = 9216$ particles

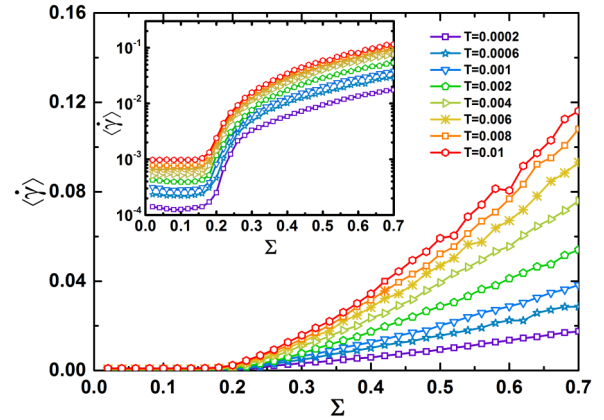


FIG. 1. Strain rate as a function of the applied stress Σ , at the steady state, for a poorly annealed system at different temperatures. The inset shows the same plot in semilogarithmic scale.

simulated at several low temperatures (see Fig. 1). We observe that the strain rate exhibits a continuous transition from a creep regime with a very small strain rate to a postyield regime with a finite strain rate. The strain rate as a function of stress exhibits a convex shape which is consistent with the velocity of elastic manifolds close to a depinning transition at finite temperatures, with the zero-temperature yielding transition in models with marginal stability [17], and also with previous simulation results obtained under constant strain rate [20].

However, the temperature dependence seems to deviate from what is observed in depinning and in amorphous solids under strain-rate control. In thermal systems exhibiting a depinning transition, it is known that close to the transition, the strain rate scales with stress and temperature according to the scaling relation [27,28]

$$\dot{\gamma} T^{-\psi} \sim \mathcal{A}(f T^{-\psi/\beta}), \quad (1)$$

where $\mathcal{A}(x)$ is a nonuniversal scaling function, β is the velocity (strain-rate) critical exponent ($\dot{\gamma} \sim f^\beta$ at zero temperature), ψ is the thermal rounding critical exponent, and

$$f = \frac{\Sigma - \Sigma_c}{\Sigma_c} \quad (2)$$

is the reduced stress normalized by a critical shear stress Σ_c . In Fig. 2 we see that for points in the vicinity of the transition we can use this relation to collapse the data on a single master curve, which indicates that the system exhibits thermal rounding typical of depinninglike critical behavior. The data collapse is obtained for $\Sigma_c \approx 0.30$, $\beta = 0.47$, and $\psi = 0.15$. However, if we use the scaling relation

$$\dot{\gamma} \sim T^\psi f^\beta, \quad (3)$$

with $\beta = 1.23(5)$, $\psi = 0.48(3)$, and $\Sigma_c = 0.17(8)$, we get a much better data collapse that covers a large range of stress values, as can be seen in Fig. 3. These values are to be compared to the range of values of β and ψ reported in the literature, where β was found to be in the range 0.3–0.8 [28–39] and ψ was found to be in the range 0.14–0.24 for depinning [28,30,35,40–42] (we are not aware of a measurement of ψ in amorphous solids). Since this scaling relation describes the

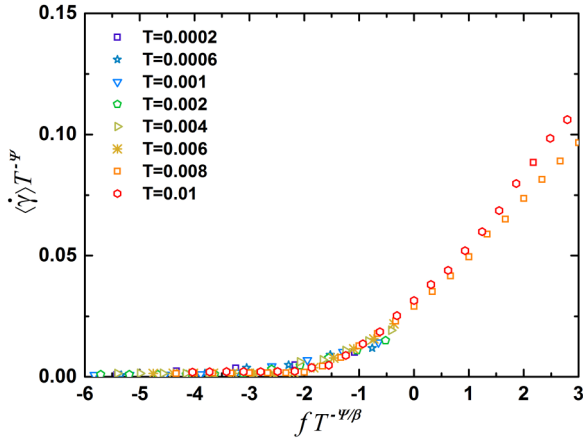


FIG. 2. Data collapse of the part of the data close to Σ_c from Fig. 1 onto a single master curve using the scaling relation (1).

behavior on a much larger range, we believe that it is the one that is more relevant for our data.

The origin of the discrepancy between the behavior that we observe and what was observed previously is that in elastic manifolds undergoing a depinning transition [35,41–43] and amorphous solids under shear at a constant strain rate [20,44] the velocity or strain rate is insensitive to the temperature for large forces or stresses. However, here we observe a different behavior where the dependence of the strain rate on temperature becomes stronger for larger stresses (Fig. 1). We believe that the main difference stems from the fact that in the constant stress simulations, we are controlling the confining pressure rather than the volume, which is typically constant in simulations under constant strain rate. This means that, contrary to most simulations performed under a constant strain rate, the material is not incompressible and the density changes during the simulation. It is known that plastic events become softer when materials are allowed to dilate (see the theoretical explanation in [45]) and the fact that the density is allowed to change means that steady states subject to different temperatures will be different even for the same applied stress.

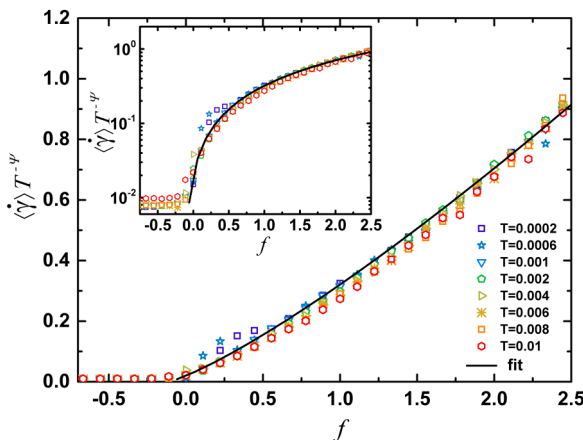


FIG. 3. Data collapse of the data from Fig. 1 onto a single master curve using the scaling relation (3). The solid line is a fit to the function af^β . The inset shows the same plot in semilogarithmic scale.

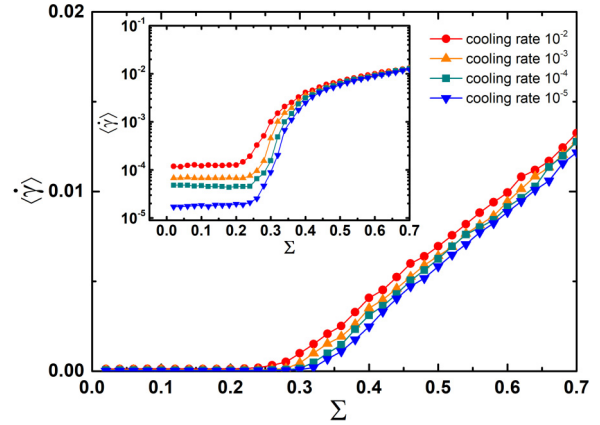


FIG. 4. Effect of the cooling rate on the steady-state strain rate at $T = 10^{-4}$. We can see that even for a very slow quench the transition from creep to a flowing phase is continuous. The inset shows the same plot in semilogarithmic scale.

We next study the effect of the quenching protocol on the asymptotic (steady-state) strain rate. We can see that even at a very low temperature $T = 1 \times 10^{-4}$ the steady state exhibits a seemingly continuous transition (Fig. 4), in contradiction to the strong effect of the quenching protocol on the yield stress in simulations at constant strain rates. Below we show that this difference stems from the effect of thermal fluctuations on the transient dynamics.

B. Effect of different quenching protocols

As we mentioned in the Introduction, the mechanical response of amorphous solids is highly dependent on the preparation protocol used, which should affect the nature of the transition. However, in the preceding section we have shown that the steady-state strain rate always exhibits a continuous transition independent of the quenching protocol. To understand this observation we study the transient dynamics. Figure 5 shows the strain rate as a function of time for different stresses (different colors) and starting from samples prepared using different initial quenches. As we can see, the quench rate has two distinct effects on the dynamics: For a slow quench [Fig. 5(a)] a larger stress is needed to obtain a flowing steady state compared to the fast quench [Fig. 5(b)] and the spacing between the different curves becomes larger. We can also observe that for stresses close to the transition for which the system eventually flows, the strain rate exhibits transient behavior which involves a temporary decrease followed by an increase, indicating a possible temporary arrest (visually, the strain rate as a function of time curves upward). We believe that this is due to the system becoming temporarily arrested by a stress-energy barrier, related to the stress peak observed in shearing of well-annealed amorphous solids, and that this barrier is eventually overcome by thermal fluctuations, which leads to the observed continuous change in the steady-state strain rate. Therefore, we conclude that for a constant stress and constant confining pressure, the preparation protocol of the initial configuration affects the transient behavior but not the transition in the steady-state strain rate, which is always continuous. In order to further

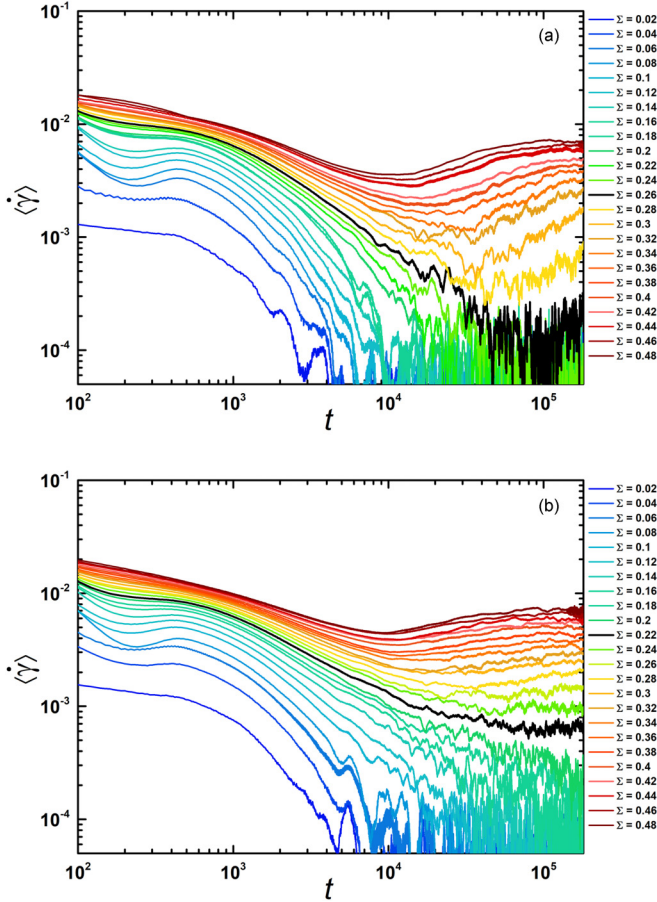


FIG. 5. Strain rate as a function of time for simulations of a binary mixture. Different colors correspond to different stresses. The stress changes (from bottom to top) from $\Sigma = 0.02$ (cold) to $\Sigma = 0.48$ (warm) in steps of 0.02. The black line represents the transient strain rate at approximately Σ_c . (a) Results for a sample prepared using the slowest quench protocol. One can see that for the slow quench, the system becomes arrested for higher stress values and exhibits a transient decrease in the strain rate followed by an increase towards the steady state. (b) Results for samples prepared using the fastest quench protocol.

compare our results to simulations performed using a constant strain rate, we also study avalanche statistics, as is discussed below.

C. Avalanche size distribution

One of the hallmarks of critical behavior is the appearance of fluctuations on all scales, which in systems exhibiting avalanches is manifested in power-law scaling of the avalanche size distribution [46]

$$D(S) \sim S^{-\tau} \mathcal{D}(-S/S_{\max}). \quad (4)$$

Here $\mathcal{D}(x)$ is a nonuniversal scaling function, which is constant for vanishing x values, S_{\max} is a cutoff avalanche size which diverges at the critical stress Σ_c for an infinite system, and τ is the avalanche size exponent. For systems under constant stress, a measure of the avalanche size is the amount of strain experienced after an event in which the system loses stability, while for a system under strain-rate control, the

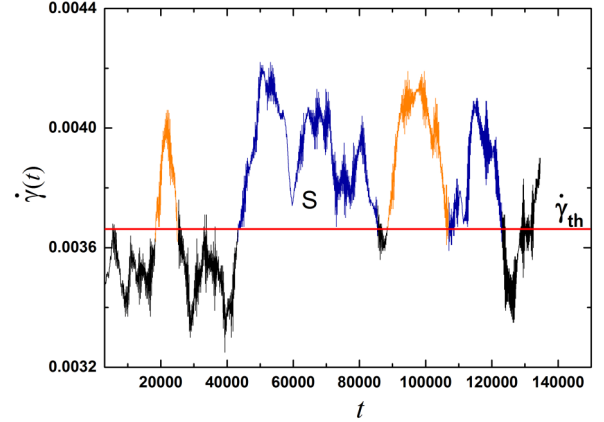


FIG. 6. Avalanche sizes obtained from the thermostated simulations. The red horizontal line represents the average strain rate $\langle \dot{\gamma} \rangle$ and the colored parts of the curve represent avalanches. An avalanche duration is the time that the strain rate spends above the average value.

avalanche size is the amount of stress released during such an event.

To extract avalanche sizes in the thermal stress-controlled systems we use thresholding; we consider as part of the avalanche only $\dot{\gamma}$ values larger than the time-averaged strain rate $\dot{\gamma}_{th} = \langle \dot{\gamma}(t) \rangle_t$. An avalanche size is then defined as the total amount of strain increase during an interval in which the strain rate is continuously larger than the average (this is illustrated in Fig. 6). This total strain increase during the avalanche is then calculated using the integral

$$S = \int_{t_1}^{t_2} [\dot{\gamma}(t) - \dot{\gamma}_{th}] dt, \quad (5)$$

where t_1 is a point in time where $\dot{\gamma}$ becomes larger than $\dot{\gamma}_{th}$ and t_2 is the first point after t_1 at which $\dot{\gamma}$ becomes lower than $\dot{\gamma}_{th}$.

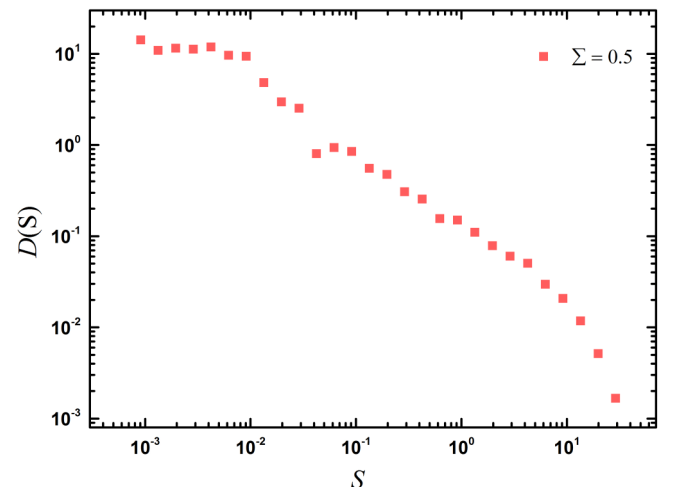


FIG. 7. Avalanche size distribution at $\Sigma = 0.5$ for $N = 9216$ at $T = 10^{-4}$.

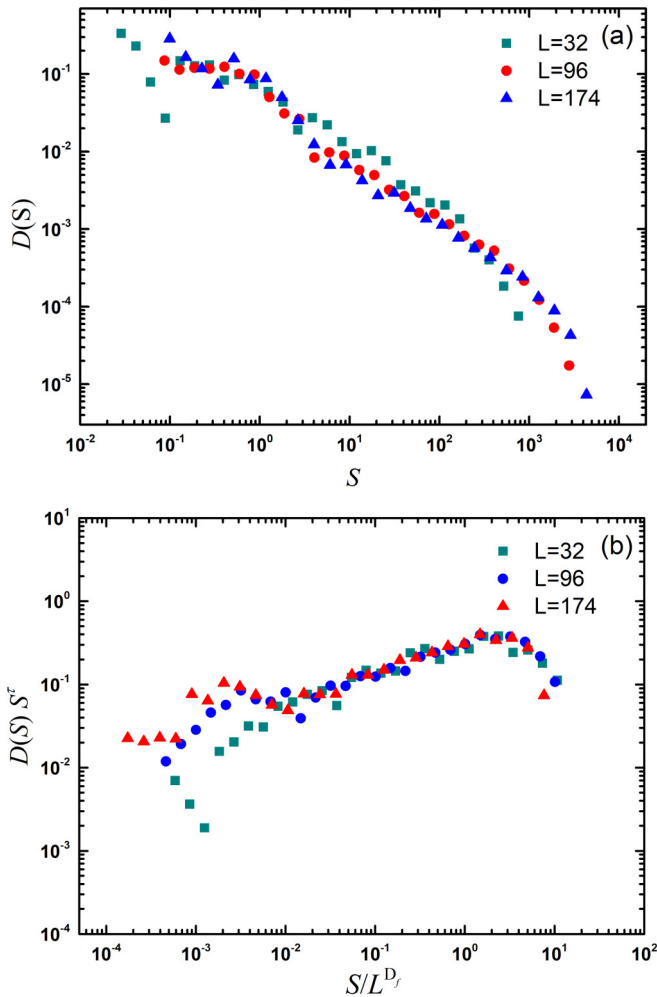


FIG. 8. (a) Avalanche size distributions for different system sizes L ($L = \sqrt{N}$ is the linear system size). (b) Finite-size scaling of the avalanche size distribution exhibiting data collapse.

As we can see in Fig. 7, we find that for $\Sigma = 0.5$ (recall that $\Sigma_c \approx 0.17$) the avalanche sizes are power-law distributed with a cutoff. To extract the exponent τ we fit the linear part of the distribution. We find $\tau = 1.20(3)$, which is similar to the values found in both overdamped molecular dynamics simulations and elastoplastic models [21,47,48]. We next study the finite-size dependence of the distribution (Fig. 8) and show that the distributions obtained for different system sizes $L = 32, 96, 174$ can be collapsed onto one master curve using the relation [49,50]

$$D(S) = S^{-\tau} \mathcal{G}(S/L^{D_f}). \quad (6)$$

The data collapse is obtained using the exponents $\tau = 1.1(3)$ and $D_f = 1.23(5)$, where the latter is the fractal dimension of the avalanches. For comparison, note that the fractal dimension was estimated to be $D_f \sim 1.1$ in elastoplastic models [48].

Our observation that the statistics under stress control are described by the same probability distribution function with similar exponents as under strain-rate control was not completely expected since typical stress-controlled avalanches

include several strain-controlled avalanches and are therefore typically larger.

III. DISCUSSION

Studying the dynamics of amorphous solids under constant stress at low temperatures, we have shown that the steady-state strain rate exhibits a continuous transition from creep to flow at a finite strain rate as a function of the stress. We have also found that for our thermal system, the continuity of the transition does not depend on the preparation of the amorphous solids from the liquid. We observed that the strain rate is a convex function of the stress, which may be a result of thermal rounding or a result of marginal stability (or both), and for systems prepared using a fast quench, we have shown that the strain rate as a function of stress, for different temperatures, can be collapsed onto one master curve. For stresses and strain rates close to yield, we collapsed the data using a scaling relation that was used to describe thermal depinning transitions, while a different scaling relation was shown to collapse the entire range of strain rate, stress, and temperatures. The different scaling behavior was ascribed to a different temperature dependence than was observed in simulations of amorphous solids with strain-rate control and we ascribed the differences to the use of NPT rather than the NVT ensemble used in simulations subject to constant strain rate. The data collapse was used to extract the strain-rate exponent β , the thermal rounding exponent ψ , and the yield stress Σ_c . We further studied the differences in the transient behavior between fast and slow quench rates and showed that for well-annealed initial configurations the transient strain rate is a nonmonotonic function of time, indicating a temporary arrest due to the existence of an energy barrier. This conclusion is in agreement with previous results that showed that the yielding transition exhibits properties of a discontinuous transition [1] and with more recent results obtained for constant strain-rate simulations at zero temperature, which were shown to exhibit a transition from brittle to ductile yielding [2]. However, we should note that in our simulations these effects were only transient and the steady-state strain rate always increased continuously from zero even for solids prepared by a slow quench. Finally, we studied the avalanche statistics at low temperatures and obtained critical exponents that are consistent with results obtained from strain-rate-controlled simulations and elastoplastic models. Further studies will focus on better understanding the origin of the differences between the temperature sensitivity observed in our stress-controlled simulations and simulations and experiments of systems under strain-rate and stress control as well as on the statistics of avalanches close to the yield point.

ACKNOWLEDGMENTS

H.X., J.C.A., and I.R. were supported by the German-Israeli Foundation through Grant No. I-2485-303.14/2017 and by the Israel Science Foundation through Grant No. 1301/17. I.R. would like to thank M. Schechter and Muhittin Mungan for useful discussions.

APPENDIX: METHODS

1. Molecular dynamics model

We simulated a 50:50 binary mixture of large and small particles interacting via Lennard-Jones potentials with system sizes of $L = 32, 96$, and 174 in two dimensions (number of particles is $N = L^2$). The interatomic potential is given by

$$V_{\alpha\beta}(r) = 4\epsilon_{\alpha\beta} \left[\left(\frac{\sigma_{\alpha\beta}}{r} \right)^{12} - \left(\frac{\sigma_{\alpha\beta}}{r} \right)^6 \right] \quad (r < r_c), \quad (\text{A1})$$

where $\alpha, \beta \in \{A, B\}$. We used $\epsilon_{AA} = \epsilon_{AB} = \epsilon_{BB} = 1.0$, $\sigma_{AA} = 1.0$, $\sigma_{AB} = 1.2$, and $\sigma_{BB} = 1.4$ and the potential is truncated and shifted at $r_c = 2.5\sigma_{\alpha\beta}$. All simulations are reported in Lennard-Jones units where time is measured with respect to $\tau = \sqrt{m\sigma^2/\epsilon}$. In all of the simulations we used the LAMMPS molecular dynamics package [51].

To prepare the initial samples from the quench, we followed a protocol that is based on standard experimental procedures used to prepare bulk metallic glasses. Our protocol followed three steps. (i) A fluid was first equilibrated at a high temperature of $T = 1.0$. (ii) The final configuration was cooled to low temperature $T = 10^{-4}$ with different cooling rates ranging from 10^{-3} (fastest) to 10^{-5} (slowest). (iii) The sample was then equilibrated at fixed low temperatures $T = 2 \times 10^{-4}, 6 \times 10^{-4}, 1 \times 10^{-3}, 2 \times 10^{-3}, 4 \times 10^{-3}, 6 \times 10^{-3}, 8 \times 10^{-3}, 1 \times 10^{-2}$ and finally quenched to zero temperature using the fast inertial relaxation engine algorithm. The system was then sheared at a finite constant temperature using Parinillo-Rahman. We tested the sensitivity of the results to the T_{damp} parameter (a parameter controlling the rate of equilibration) and found that it did not significantly affect the results for values less than 100 times the time step. We therefore set T_{damp} equal to ten times the time step.

2. Constant stress molecular dynamics simulations

In order to apply a constant stress, we use a LAMMPS implementation of the method suggested by Parrinello and Rahman [25]. Here we provide a brief description of this method. In the Parrinello-Rahman algorithm, the particles are subject

to periodic boundary conditions confining them to reside on a parallelogram-shaped cell with a shape that is defined by the two vectors $(\hat{\ell}_1, \hat{\ell}_2)$, where each vector $\hat{\ell}_i$ represents the direction and the length of an edge of the simulation parallelogram. The deformation of the system is represented by the matrix $L = [\hat{\ell}_1, \hat{\ell}_2]$, where each $\hat{\ell}_i$ is a column vector of the matrix. In order to allow the system to become strained and reach the target stress, the matrix L (and thus the shape and size of the simulation cell) is allowed to vary. The strain is calculated by comparing L to a reference state $L^0 = [\hat{\ell}_1^0, \hat{\ell}_2^0]$. The relation between the reference and current configuration is given by the strain gradient matrix $F : L = FL^0$, which also provides a connection between the coordinates x in the actual configuration and coordinates X at the reference (prestrained) configuration $x = FX$, assuming a constant strain along the simulation box. The vectors $\hat{\ell}_i$ are used to scale the coordinates and momenta $r_i = Ls_i$ and $p_i = L\pi_i$. These, as well as the deformation gradient and the volume, are then used in the modified Hamiltonian

$$\begin{aligned} \mathcal{H} = & \mathcal{V}_N(\dots, FL^0 s_i, \dots) + \sum_{i=1}^N \frac{(FL^0 \pi_i) \cdot (FL^0 \pi_i)}{2m_i} \\ & + \frac{\prod \cdot \prod}{2M} - \frac{1}{2} V_0 (\sigma_{ij} + p \delta_{ij}) (F^T F - \mathcal{J})_{ij} - p(V - V^0), \end{aligned} \quad (\text{A2})$$

where M is a masslike quantity that gives ‘‘inertia’’ to the strain gradient F , V^0 is the volume, σ_{ij} is the external stress applied on the system, and p is the applied hydrostatic pressure. Hamilton’s equations for the scaled particle positions and momenta as well as the deformation gradient and its ‘‘momentum’’

$$\dot{s}_i = \frac{\partial \mathcal{H}}{\partial \pi_i}, \quad \dot{\pi}_i = -\frac{\partial \mathcal{H}}{\partial s_i}, \quad \dot{F}_i = \frac{\partial \mathcal{H}}{\partial \Pi}, \quad \dot{\Pi} = -\frac{\partial \mathcal{H}}{\partial F_i} \quad (\text{A3})$$

are then solved for the predecided stress, pressure, and temperature. Here we used a variant of this algorithm (also implemented in LAMMPS) which controls the Cauchy stress rather than the Piola-Kirchhoff stress [26].

-
- [1] P. K. Jaiswal, I. Procaccia, C. Rainone, and M. Singh, *Phys. Rev. Lett.* **116**, 085501 (2016).
- [2] M. Ozawa, L. Berthier, G. Biroli, A. Rosso, and G. Tarjus, *Proc. Natl. Acad. Sci. USA* **115**, 6656 (2018).
- [3] D. Fiocco, G. Foffi, and S. Sastry, *Phys. Rev. E* **88**, 020301(R) (2013).
- [4] T. Kawasaki and L. Berthier, *Phys. Rev. E* **94**, 022615 (2016).
- [5] N. C. Keima and P. E. Arratia, *Soft Matter* **9**, 6222 (2013).
- [6] K. Hima Nagamanasa, S. Gokhale, A. K. Sood, and R. Ganapathy, *Phys. Rev. E* **89**, 062308 (2014).
- [7] S. Slotterback, M. Mailman, K. Ronaszegi, M. van Hecke, M. Girvan, and W. Losert, *Phys. Rev. E* **85**, 021309 (2012).
- [8] I. Regev, T. Lookman, and C. Reichhardt, *Phys. Rev. E* **88**, 062401 (2013).
- [9] I. Regev, J. Weber, C. Reichhardt, K. A. Dahmen, and T. Lookman, *Nat. Commun.* **6**, 8805 (2015).
- [10] P. Leishangthem, A. D. Parmar, and S. Sastry, *Nat. Commun.* **8**, 14653 (2017).
- [11] I. Regev and T. Lookman, *J. Phys.: Condens. Matter* **31**, 045101 (2018).
- [12] R. Dasgupta, H. G. E. Hentschel, and I. Procaccia, *Phys. Rev. Lett.* **109**, 255502 (2012).
- [13] C. Rainone, P. Urbani, H. Yoshino, and F. Zamponi, *Phys. Rev. Lett.* **114**, 015701 (2015).
- [14] A. H. Clark, J. D. Thompson, M. D. Shattuck, N. T. Ouellette, and C. S. O’Hern, *Phys. Rev. E* **97**, 062901 (2018).
- [15] P. Nath, S. Ganguly, J. Horbach, P. Sollich, S. Karmakar, and S. Sengupta, *Proc. Natl. Acad. Sci. USA* **115**, E4322 (2018).
- [16] V. S. Reddy, P. Nath, J. Horbach, P. Sollich, and S. Sengupta, *Phys. Rev. Lett.* **124**, 025503 (2020).
- [17] J. Lin, E. Lerner, A. Rosso, and M. Wyart, *Proc. Natl. Acad. Sci. USA* **111**, 14382 (2014).

- [18] K. A. Dahmen, Y. Ben-Zion, and J. T. Uhl, *Phys. Rev. Lett.* **102**, 175501 (2009).
- [19] J. P. Sethna, M. K. Bierbaum, K. A. Dahmen, C. P. Goodrich, J. R. Greer, L. X. Hayden, J. P. Kent-Dobias, E. D. Lee, D. B. Liarte, X. Ni *et al.*, *Annu. Rev. Mater. Res.* **47**, 217 (2017).
- [20] J. Chatteraj, C. Caroli, and A. Lemaître, *Phys. Rev. Lett.* **105**, 266001 (2010).
- [21] K. M. Salerno, C. E. Maloney, and M. O. Robbins, *Phys. Rev. Lett.* **109**, 105703 (2012).
- [22] L. Boué, H. G. E. Hentschel, I. Procaccia, I. Regev, and J. Zylberg, *Phys. Rev. B* **81**, 100201(R) (2010).
- [23] I. Srivastava, L. E. Silbert, G. S. Grest, and J. B. Lechman, *Phys. Rev. Lett.* **122**, 048003 (2019).
- [24] R. Cabriolu, J. Horbach, P. Chaudhuri, and K. Martens, *Soft Matter* **15**, 415 (2019).
- [25] M. Parrinello and A. Rahman, *J. Appl. Phys.* **52**, 7182 (1981).
- [26] R. E. Miller, E. B. Tadmor, J. S. Gibson, N. Bernstein, and F. Pavia, *J. Chem. Phys.* **144**, 184107 (2016).
- [27] D. S. Fisher, *Phys. Rev. B* **31**, 1396 (1985).
- [28] A. A. Middleton, *Phys. Rev. B* **45**, 9465 (1992).
- [29] P. Paruch, T. Giamarchi, and J.-M. Triscone, *Phys. Rev. Lett.* **94**, 197601 (2005).
- [30] L. W. Chen and M. C. Marchetti, *Phys. Rev. B* **51**, 6296 (1995).
- [31] P. Le Doussal, K. J. Wiese, and P. Chauve, *Phys. Rev. B* **66**, 174201 (2002).
- [32] T. Nattermann, S. Stepanow, L.-H. Tang, and H. Leschhorn, *J. Phys. (France) II* **2**, 1483 (1992).
- [33] U. Nowak and K. D. Usadel, *Europhys. Lett.* **44**, 634 (1998).
- [34] S. Lemerle, J. Ferré, C. Chappert, V. Mathet, T. Giamarchi, and P. Le Doussal, *Phys. Rev. Lett.* **80**, 849 (1998).
- [35] M. B. Luo and X. Hu, *Phys. Rev. Lett.* **98**, 267002 (2007).
- [36] M. J. Alava, P. K. V. V. Nukala, and S. Zapperi, *Adv. Phys.* **55**, 349 (2006).
- [37] O. Duemmer and W. Krauth, *Phys. Rev. E* **71**, 061601 (2005).
- [38] X. Du, G. Li, E. Y. Andrei, M. Greenblatt, and P. Shuk, *Nat. Phys.* **3**, 111 (2007).
- [39] F. Lacombe, S. Zapperi, and H. J. Herrmann, *Phys. Rev. B* **63**, 104104 (2001).
- [40] D. Vandembroucq, R. Skoe, and S. Roux, *Phys. Rev. E* **70**, 051101 (2004).
- [41] S. Bustingorry, A. B. Kolton, and T. Giamarchi, *Europhys. Lett.* **81**, 26005 (2008).
- [42] S. Bustingorry, A. B. Kolton, and T. Giamarchi, *Phys. Rev. E* **85**, 021144 (2012).
- [43] E. E. Ferrer, S. Bustingorry, A. B. Kolton, and A. Rosso, *C. R. Phys.* **14**, 641 (2013).
- [44] J. Lu, G. Ravichandran, and W. L. Johnson, *Acta Mater.* **51**, 3429 (2003).
- [45] X. Cao, A. Nicolas, D. Trimcev, and A. Rosso, *Soft Matter* **14**, 3640 (2018).
- [46] K. A. Dahmen, Y. Ben-Zion, and J. T. Uhl, *Nat. Phys.* **7**, 554 (2011).
- [47] M. Talamali, V. Petäjä, D. Vandembroucq, and S. Roux, *Phys. Rev. E* **84**, 016115 (2011).
- [48] B. Tyukodi, D. Vandembroucq, and C. E. Maloney, *Phys. Rev. E* **100**, 043003 (2019).
- [49] K. Christensen and N. R. Moloney, *Complexity and Criticality* (World Scientific, Singapore, 2005), Vol. 1.
- [50] T. Hwa and M. Kardar, *Phys. Rev. A* **45**, 7002 (1992).
- [51] S. Plimpton, *J. Comput. Phys.* **117**, 1 (1995).